Electrochemical impedance spectroscopy, another arrow in the arsenal to study the biodegradability of two-dimensional materials

*Livia Didonè,[a] Yunseok Shin,[a] Alessandro Silvestri,[c,#] Maurizio Prato,[c,d] Sungjin Park,[b] Alberto Bianco[a,]**

[a]CNRS, UPR3572, Immunology, Immunopathology and Therapeutic Chemistry, ISIS, University of Strasbourg, 67000 Strasbourg, France
E-mail: a.bianco@ibmc-cnrs.unistra.fr
[b]Department of Chemistry and Chemical Engineering, Inha University, 100 Inha-ro, Nam-gu, Incheon 22212, Korea
[c]Center for Cooperative Research in Biomaterials (CIC biomaGUNE), Basque Research and Technology Alliance (BRTA), Paseo de Miramón 194, 20014 Donostia San Sebastián, Spain
[d]Ikerbasque, Basque Foundation for Science, 48013 Bilbao, Spain

ELECTRONIC SUPPLEMENTARY INFORMATION

Materials and methods

Synthesis of CN_{Urea}

Urea (1 g, 99.0%, Sigma-Aldrich) was added to an alumina crucible then the crucible was put in a quartz tube furnace (TFP-80-3, Dongseo Science Co., Ltd., south Korea). The furnace was filled with air/H_2O gas, and the temperature was elevated to 550 ℃ with a heating rate of 10 ℃/min. The temperature was held at 550 ℃ for 4 h under a flow of air/H_2O gas. The product (CN_{Urea}, 93 mg) was obtained as yellowish powder.

Synthesis of $oxCN_{Mel}$

Melamine (1 g, 99%, Sigma-Aldrich) was added to an alumina crucible then the crucible was put in a quartz tube furnace. The furnace was filled with N_2 gas and the temperature was elevated to 550 ℃ with a heating rate of 10 ℃/min. The temperature was held at 550 ℃ for 4 h under a flow of N_2 gas. The product (CN_{Mel}, 264 mg) was obtained as yellowish powder.

CN_{Mel} (4 g) was added to a flask filled with H_2SO_4 (100 mL, 95%, Daejung). Then $KMnO_4$ (4.28 g, 99.3%, Daejung) was then slowly added to the flask in an ice-bath. The mixture was stirred for 2 h at 35 ℃ then excess water was added to the mixture in an ice-bath. H_2O_2 (35%, Junsei) was then slowly added to the mixture at 25 ℃ until no gas was evolved. The resulting mixture was filtered, washed with 1 L of 5% HCl solution followed by water-washing several times. After drying under vacuum at 25 ℃ for 12 h, $oxCN_{Mel}$ (48 mg) was obtained.

Degradation protocol of the photo-Fenton reaction

In quartz tubes has been put 0.31 mL material (CN_{Urea} and $oxCN_{Mel}$) in aqueous solution (0.78 mg/mL), 10 µL of 1 mM $FeCl_3 \cdot 6H_2O$, 2.46 mL of H_2O. Then the solution was adjusted with 0.1 M HCl, to obtain pH 4. Every 10 hours 50 µL of 100 mM H_2O_2 were injected. Every 35 hours there was the addition of 10 µL of 1 mM $FeCl_3 \cdot 6H_2O$. The reaction has been carried out for 100 hours, taking aliquots of 50 µL at times 0 h, 20 h, 50 h, and 100 h, stored at -20 °C in the dark until characterization by different techniques. Three control reactions containing 0.31 mL of material (0.78 mg/mL) and 2.46 mL of water were performed under the UV lamp, without the use of all the other catalysts.

Transmission electron microscopy

For the TEM characterizations, 6 µL of each solution has been deposited on carbon-coated copper grids, dried and analyzed on a Hitachi H7500 microscope (Tokyo, Japan) with an accelerating voltage of 80kV, equipped with an AMT Hamamatsu camera (Tokyo, Japan). TEM images in SI were obtained using a field-emission transmission electron microscope (JEM2100F, JEOL, Japan) at 200 kV using a carbon/copper holey grid (HC200eCu, EMS, USA).

Raman spectroscopy

Raman analysis of all the samples was performed using Raman spectra Renishaw inVia microRaman, equipped with 532 nm laser and a Leica microscope.

X-Ray photoelectron spectroscopy

XPS was performed on a K-ALPHA Surface Analysis Spectrophotometer (Thermo Scientific) with a basic chamber pressure of 10^{-8}-10^{-9} bar and an Al anode as X-Ray source (1486 eV). For each sample, three spectra were collected. The powder of the raw materials, pressed on copper scotch tape, was analyzed. To check the trends of the different degradation reactions, the samples were prepared by drop-casting on a Silica wafer (4 µL drop, repeated 3 to 4 times to reach a sufficient thickness). A spot size of 400 µm was chosen for the analysis. The survey spectra were the result of the average of 10 scans with a pass energy of 200.00 eV and a step size of 1 eV. The high-resolution spectra were an average of 10 scans with a pass energy of 50 eV and a step size of 0.1 eV. An electron flood gun was working during the analysis as a charge neutralizer. Deconvolution parameters: C1s spectra were deconvoluted in C=O/C=N (287.6-289.9 eV), which are partially overlapping one another; C-O/C-N (286.2-287.2 eV), in this case, was considered a range of error too, since the binding energies of the two types of bonds were overlapped; C-C (284.4-285.3 eV) for sp^2 and sp^3 carbon atoms. For data analysis casaXPS (2.3.18) software was used: A Shirley background subtraction was applied; a lineshape 70% Gaussian/30% Lorentzian [GL(30)] was selected; the FWHM was constrained to be the same for all peaks, apart from the pi*peak because it is a broad signal, and for the C-N/C-S bond because this peak overlapped with C-O and C-C.

X-ray diffraction

XRD patterns were measured using a DMAX-2500 diffractometer (Rigaku, Tokyo, Japan).

Fourier transform infrared spectroscopy

FT-IR spectra were obtained from KBr pellets containing the samples using an FT-IR vacuum spectrometer (Bruker VERTEX 80 V, Bruker, Germany).

Photoluminescence

PL spectra (f = 0.5 m, Acton Research Co., Spectrograph 500i, USA) were performed at room temperature with a 300 nm diode-pumped solid-state laser excitation using an intensified charge-coupled device (PI-MAX3) (Princeton Instrument Co., IRY1024, USA)

Electrical impedance spectroscopy

EIS was registered using an Autolab MSTAT204 potentiostat/galvanostat (Metrohm). A three-electrode configuration, composed by GCE as a working electrode (WE), Pt mesh as a counter electrode (CE), and an Ag/AgCl reference electrode (RE), was employed. 10 µl of C_3N_4 suspensions (1mg/ml) were drop-casted onto the WE (electrode area 0.07 cm^2). Measurements were performed in a

5 mM solution of potassium hexacyanoferrate (III) using as an electrolyte 100 mM PBS buffer (containing 100 mM KCl, Ph 7.4), A potential of 0.21 V (vs. reference) was applied with a perturbation of 10 mV, in the frequency range between 100 kHz and 10 mHz. The fitting of EIS data was performed using NOVA software v2.1.6 (Metrohm AutoLab B.V.). In the case of the time-resolved measurements, the same conditions were employed, but 10 µl of 0.1 mg/ml C_3N_4 suspensions were drop cast on the GCE.

Characterizations of CN_{Urea} and $oxCN_{Mel}$ materials

As shown in the TEM images in Figure S1), CN_{Urea} and $oxCN_{Mel}$ powder samples are characterized by small overlapped flakes.

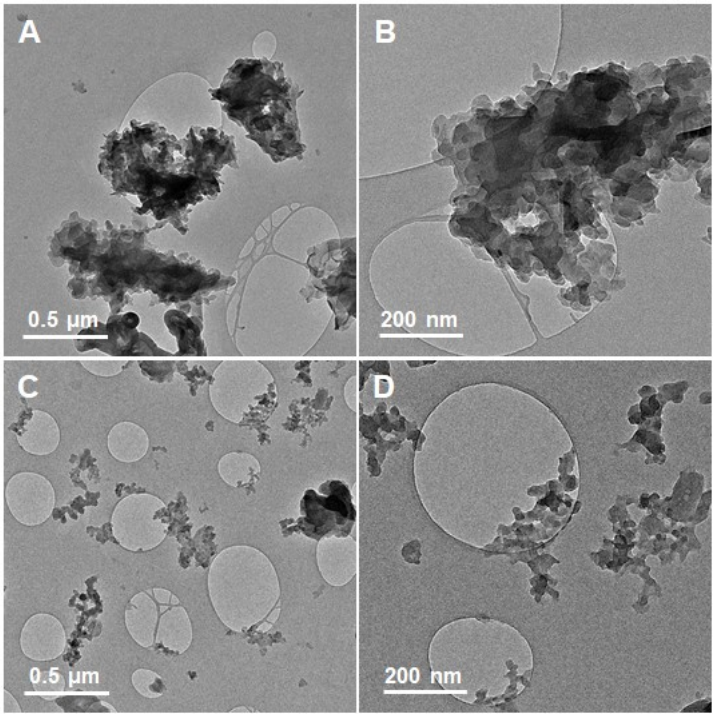

Figure S1. TEM images of powder samples: A), B) CN_{Urea} and C), D) $oxCN_{Mel}$.

The chemical structures of CN_{Urea} and $oxCN_{Mel}$ were futher investigated by X-ray diffraction (XRD), X-ray photoelectron spectroscopy (XPS), and Fourier transformed infrared (FT-IR) spectroscopy. The amount of elemental O in $oxCN_{Mel}$ powder, as measured by XPS, resulted much higher than that of CN_{Urea} (Table S1). This feature indicates the introduction of oxygen-containing functionalities during the oxidation process.

Table S1. Elemental composition of CN_{Urea} and $oxCN_{Mel}$, measured by XPS.

Sample	C (at%)	N (at%)	O (at%)
CN_{Urea}	46.6	52.2	1.2
$oxCN_{Mel}$	31.7	37.8	30.5

The XRD is a common fingerprint to determine the formation of C_3N_4 network containing tri-s-triazine units. The XRD patterns of both samples show two major peaks at ~13° and ~27°, corresponding to an intralayer distance between tri-*s*-triazine rings and an interlayer distance, respectively (Figure S2).[1]

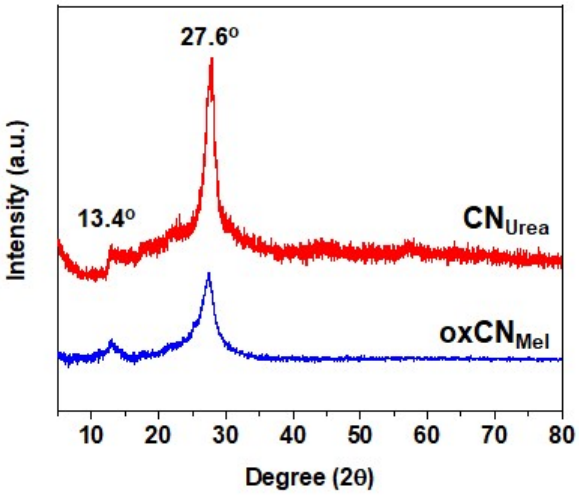

Figure S2. XRD patterns of CN_{Urea} and $oxCN_{Mel}$.

The suspensions of both samples in water showed fluorescence under irradiation using UV light and photoluminescence (PL) properties, obtained with an excitation of 300 nm (Figure S3). This PL feature is one of the common properties of C_3N_4 structures. However, the PL wavelength of $oxCN_{Mel}$ shifted to the lower wavelenght relative to that of CN_{Urea}. These PL data suggest that $oxCN_{Mel}$ possesses a different chemical structure from CN_{Urea}.

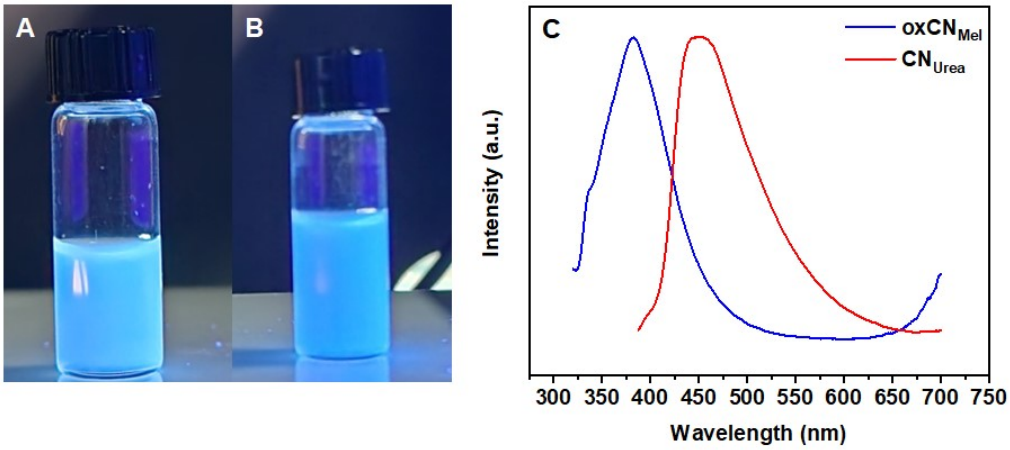

Figure S3. Fluorescent images of A) CN_{Urea} and B) $oxCN_{Mel}$. C) Photoluminescence spectra of CN_{Urea} and $oxCN_{Mel}$ excited at 300 nm.

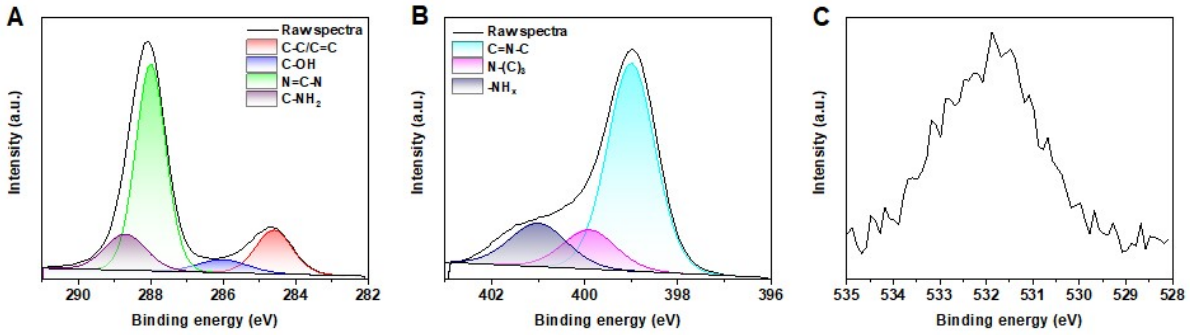

Figure S4. Deconvoluted high resolution XPS spectra of CN_{Urea}; A) C 1s, B) N 1s, and C) O 1s.

The XPS C and N 1*s* spectra of CN_{Urea} show a typical pattern for C_3N_4-based materials, revealing the formation of the C_3N_4 network (Figure 4A). The deconvoluted C 1s spectra have peaks at 284.6, 286.0, 287.0, 288.0, and 288.7 eV which correspond to C=C/C-C, C-O, N=C-N in tri-*s*-triazine rings, and C-NH_2 moieties, respectively (Figure S4). In the deconvoluted N 1s spectra, peaks at 399.0, 399.9, and 401.0 eV correspond to C-N=C, N-$(C)_3$, and NH_x groups, respectively (Figure S4B).[2] Trace of O atoms are also observed (Figure S4C). Although C_3N_4 materials that are completely condensed are not expected to exhibit an XPS peak at 284.6 eV for C=C/C-C, this peak has frequently been observed as a minor peak in previous studies, suggesting the presence of C impurities in the synthesized C_3N_4 materials.[3] This is a reason why larger amounts of C atoms were observed in the samples relative to that of theoretical C_3N_4 structures. XPS spectra of $oxCN_{Mel}$ are different from those of CN_{Urea}. The intensities of the peaks corresponding to the C(=O)O/C=O (XPS C 1s) and N–Hx groups (XPS N 1s) of $oxCN_{Mel}$ increased relative to that of CN_{Urea} (Figure S5). The N 1s peak for C=N-C group decreased after oxidation.

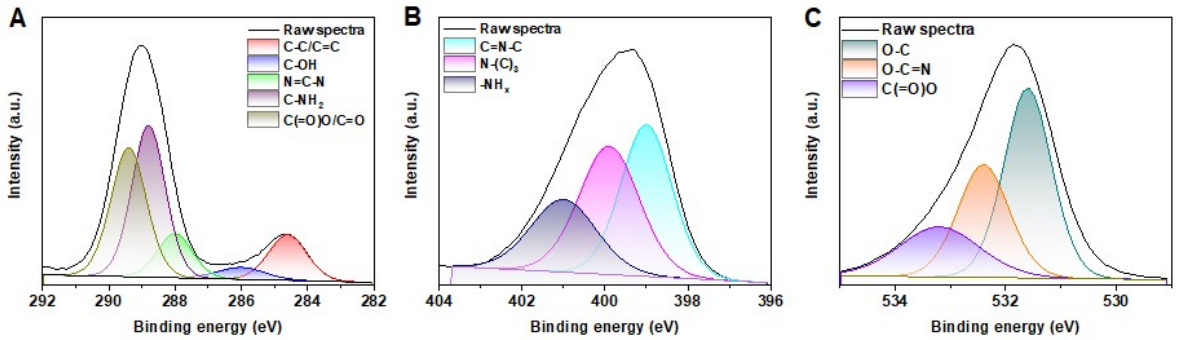

Figure S5. Deconvoluted high resolution XPS spectra of $oxCN_{Mel}$; A) C 1s, b) N 1s, and C) O 1s.

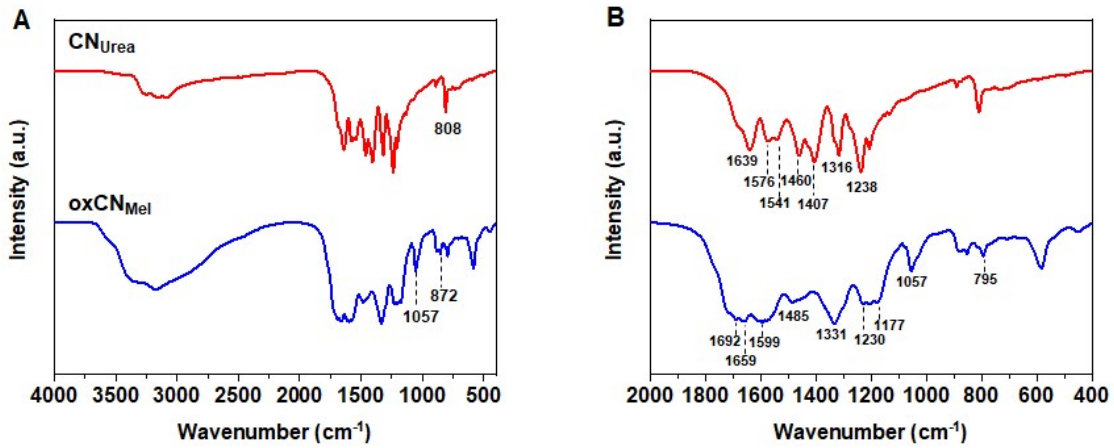

Figure S6. FT-IR spectra of CN_{Urea} and $oxCN_{Mel}$. A) Full range between 4000 and 400 cm^{-1} and B) selected range between 2000 and 400 cm^{-1}.

The FT-IR spectrum of CN_{Urea} shows typical features of C_3N_4 materials (Figure S6). Peaks at 1407, 1316, 1238 and 808 cm^{-1}, corresponding to a breathing mode of triazine rings, secondary bridging amines, and a C-N stretching of the tertiary nitrogen groups in tri-*s*-triazine rings, respectively (Figure S6). The peaks at 1639, 1576, 1541, 1460 and cm^{-1} correspond to the stretching modes of the tri-*s*-triazine ring. The broad bands between 3300 and 3000 cm^{-1} correspond to terminal/bridging amino groups (-NH_2 or -NH- groups). The spectrum of $oxCN_{Mel}$ shows stronger peaks around 3300 – 3000 and 1600 – 1700 cm^{-1}, corresponding to -NH_2/-NH- and C(=O)O/C=O groups, than that of CN_{Urea}. These spectra features indicate that the oxidatinn process forms -NH_2/-NH- and C(=O)O/C=O groups at the edge of $oxCN_{Mel}$ materials. The functional groups could be generated by decomposition of the N–C=N groups at the edges of the C_3N_4 networks during oxidation.[4]

Tyndall effect

To confirm the presence of fragments in the solutions both at the beginning and at the end of the degradation reaction, the Tyndall effect has been settled. This phenomenon is a light-scattering effect that appears when particles suspended in a medium are larger than the wavelength of light (650 nm) crossing the solution.[5] As descried by the red laser line, the presence of particles is constant for CN_{Urea} but, in comparison to the result obtained analyzing the first material, the Tyndall effect for $oxCN_{Mel}$ resulted less evident, suggesting the presence of fewer particles (Figure S7).

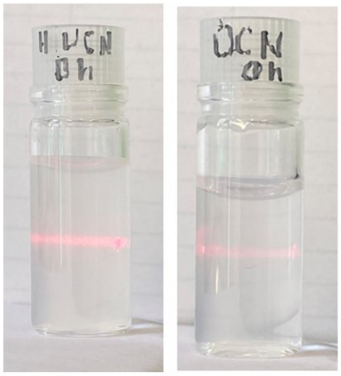

Figure S7. Tyndall effect of CN_{Urea} and $oxCN_{Mel}$.

A

$$Fe^{3+} + H_2O_2 + h\nu \rightarrow Fe^{3+}OOH + H^+ \quad (1)$$

$$Fe^{3+}OOH \rightarrow Fe^{2+} + \text{•}OOH \quad (2)$$

$$Fe^{2+} + H_2O_2 \rightarrow Fe^{3+} + \text{•}OH + OH^- \quad (3)$$

$$Fe(OH)^{2+} + h\nu \rightarrow Fe^{2+} + \text{•}OH \quad (4)$$

$$H_2O_2 + h\nu \rightarrow 2(\text{•}OH) \quad (5)$$

B

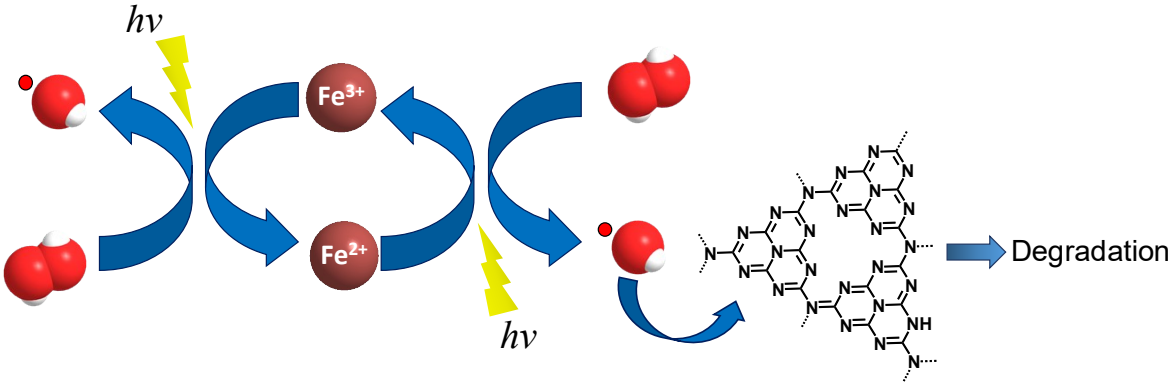

Figure S8. Equations involved in the generation of hydroxyl radicals during the photo-Fenton reaction (A), leading to the degradation of carbon nitrides (B).

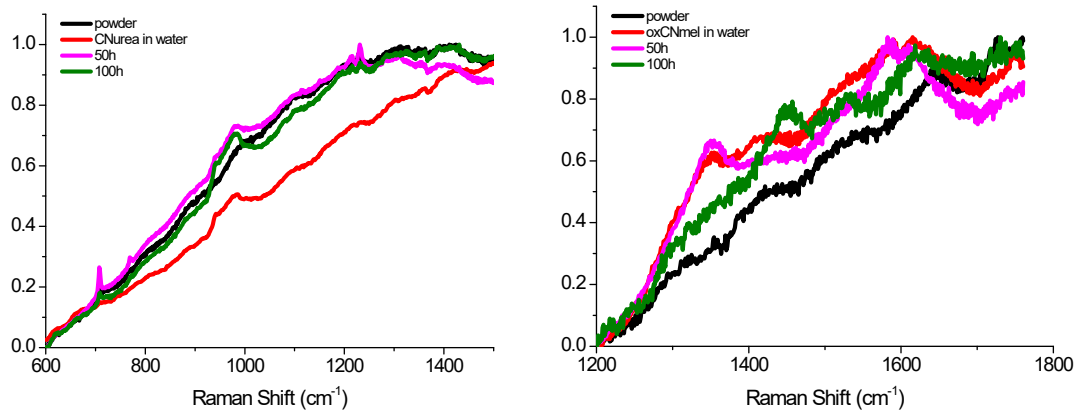

Figure S9. Raman spectra of CN_{Urea} (A) and $oxCN_{Mel}$ (B) at different time points during the photo-Fenton process.

Even if the materials were analyzed either depositing their powder or drying the dispersions at the different time points on the silica wafer, CN_{Urea} and $oxCN_{Mel}$ were highly autofluorescent masking their characteristic peaks. C_3N_4 are recognizable thanks to a peak at 707 cm^{-1}, attributed to the heptazine ring, and to a second peak at 1232 cm^{-1}, which represents the stretching vibration mode of C-N heterocycles.[6] In the spectra obtained from the analysis, these two characterizing peaks were very weak if not absent, thus hampering the observation of their evolution during the degradation process.

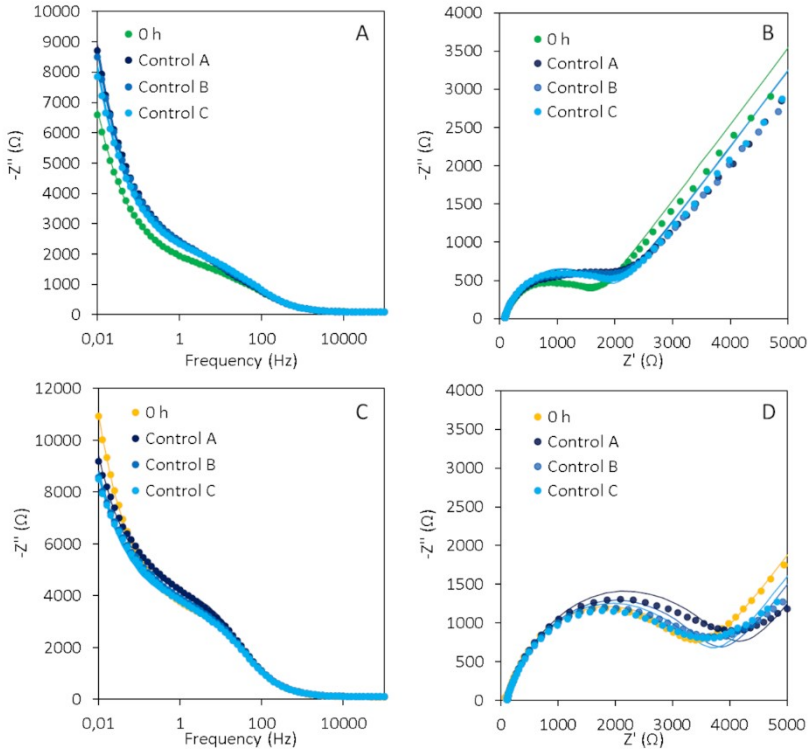

Figure S10. A) Bode plot of CN_{Urea} before the photo-Fenton reaction (0 h) and after the control reactions (Control A: with UV lamp, with Fe, without H_2O_2; Control B: with UV lamp, without Fe, without H_2O_2; Control C: with UV lamp, without Fe, with H_2O_2). The dots represent the experimental data, the line the fitting. B) Nyquist plot of CN_{Urea} before the photo-Fenton reaction (0 h) and after the control reactions. C) Bode plot of $oxCN_{Mel}$ before the photo-Fenton reaction (0 h) and after the control reactions. D) Nyquist plot of $oxCN_{Mel}$ before the photo-Fenton reaction (0 h) and after the control reactions.

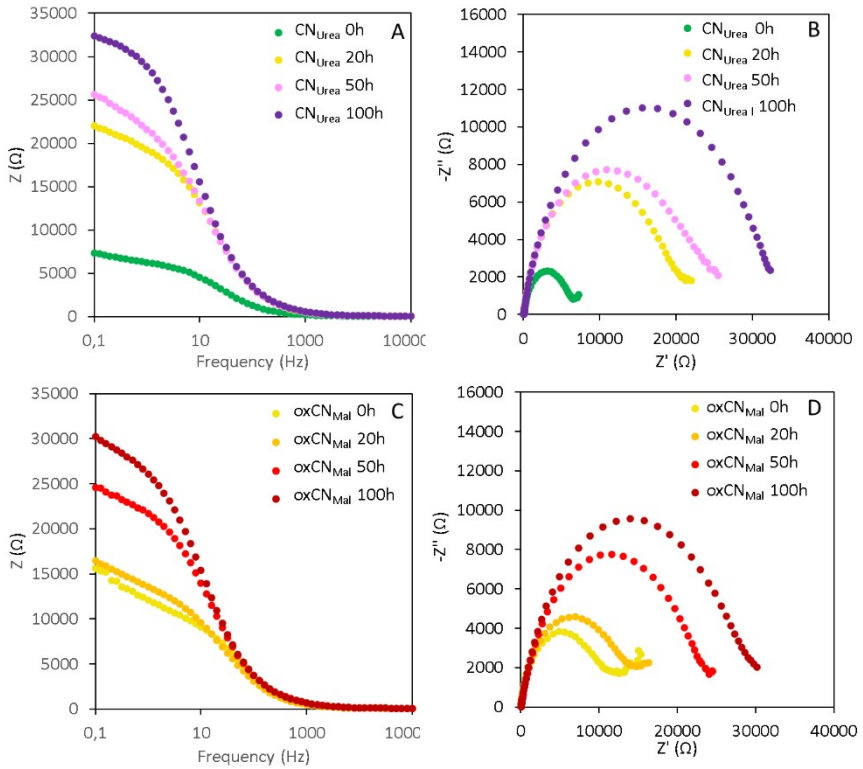

Figure S11. EIS measurements were obtained by drop casting 0.1 mg/ml of C_3N_4 on a GCE electrode, in a solution of 5 mM of $K_3[Fe(CN)_6]$. A potential of 0.21 V (vs. reference) was applied with a perturbation of 10 mV in a range of frequencies between 100 kHz and 10 mHz. A) Bode plot of CN_{Urea} at different time points (0, 20, 50, and 100 h) of the photo-Fenton reaction. B) Nyquist plot of CN_{Urea} at different time points (0, 20, 50, and 100 h) of the photo-Fenton reaction. C) Bode plot of $oxCN_{Mel}$ at different time points (0, 20, 50, and 100 h) of the photo-Fenton reaction. D) Nyquist plot of $oxCN_{Mel}$ at different time points (0, 20, 50, and 100 h) of the photo-Fenton reaction

References

1) J. Oh, Y. Shim, S. Lee, S. Park, D. Jang, Y. Shin, S. Ohn, J. Kim and S. Park, *J. Solid State Chem.*, 2018, **258**, 559–565.

2) J. Oh, J. M. Lee, Y. Yoo, J. Kim, S. J. Hwang and S. Park, *Appl. Catal. B*, 2017, **218**, 349–358.

3) D. Jang, S. Jeon, E. Y. Shin and S. Park, *Carbon Lett.*, 2023, **33**, 803–809.

4) J. Oh, R. J. Yoo, S. Y. Kim, Y. J. Lee, D. W. Kim and S. Park, *Chem. Eur. J.*, 2015, **21**, 6241–6246.

5) J. Stetefeld, S. A. McKenna and T. R. Patel, *Biophys Rev.*, 2016, **8**, 409–427.

6) M. Wang, F. Ma, Z. Wang, D. Hu, X. Xu and X. Hao, *Photonics Res*, 2018, **6**, 307.